ACSNANO

www.acsnano.org

Versatile Triboiontronic Transistor *via* Proton Conductor

Xixi Yang,[Δ] Jing Han,[Δ] Jinran Yu,[Δ] Youhui Chen, Huai Zhang, Mei Ding, Chuankun Jia, Jia Sun, Qijun Sun,* and Zhong Lin Wang*

Cite This: https://dx.doi.org/10.1021/acsnano.0c03030

Read Online

ACCESS | Metrics & More | Article Recommendations | Supporting Information

ABSTRACT: Iontronics are effective in modulating electrical properties through the electric double layers (EDLs) assisted with ionic migration/arrangement, which are highly promising for unconventional electronics, ionic sensory devices, and flexible interactive interface. Proton conductors with the smallest and most abundant protons (H^+) can realize a faster migration/polarization under electric field to form the EDL with higher capacitance. Here, a versatile triboiontronic MoS_2 transistor *via* proton conductor by sophisticated combination of triboelectric modulation and protons migration has been demonstrated. This device utilizes triboelectric potential originated from mechanical displacement to modulate the electrical properties of transistors *via* protons migration/accumulation. It shows superior electrical properties, including high current on/off ratio over 10^6, low cutoff current (~0.04 pA), and steep switching properties (89 μm/dec). Pioneering noise tests are conducted to the tribotronic devices to exclude the possible noise interference introduced by mechanical displacement. The versatile triboiontronic MoS_2 transistor *via* proton conductor has been utilized for mechanical behavior derived logic devices and an artificial sensory neuron system. This work represents the reliable and effective triboelectric potential modulation on electronic transportation through protonic dielectrics, which is highly desired for theoretical study of tribotronic gating, active mechanosensation, self-powered electronic skin, artificial intelligence, *etc.*

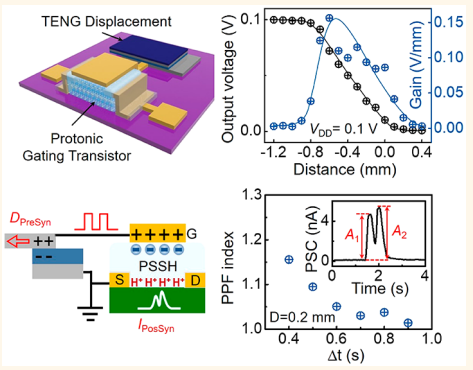

KEYWORDS: *triboiontronic transistor, proton conductor, triboelectric nanogenerator, logic inverter, sensory neuron*

Iontronic devices, which utilize ionic migration and arrangement to effectively modulate electronic properties, have evoked interdisciplinary research with involved ion-electronic coupling from interface electrochemistry,[1,2] unconventional electronics,[3] solid-state physics,[4,5] and even bio-inspired sciences/technology,[6] *etc.* Relying on the rapid migration of ions under an electric field, the space charges strongly accumulate at the interface of ionic electrolyte and active materials to form the electric double layer (EDL) with ultrahigh capacitance (>1 $\mu F \cdot cm^{-2}$), which is beneficial for advanced ionic artificial skin,[7−9] soft interactive interface,[10,11] electrochromic cells,[1] and energy-harvesting devices.[12] Specifically, the induced electric field in EDL field effect transistors (EDL-FETs) can reach as high as 30 $MV \cdot cm^{-1}$,[13] which shows great potential in the modulation of charge-carrier transport,[14] phase control of nanomaterials,[15,16] gate-optimization of thermoelectrics,[17] and neuromorphic devices.[18−20] Recently emerging triboiontronics, taking advantage of Maxwell's displacement current from triboelectric nanogenerator (TENG)[21,22] as the gate driving force, efficiently bridges the triboelectric potential modulation on charge carrier transport mediated with ion migration. It offers a versatile platform to realize mechanical behavior derived high performance electronic devices and multifunctional sensors.[23] A high performance tribotronic MoS_2 transistor has been demonstrated to operate in an active mode with low threshold displacement at 75 μm and steep switch properties of 20 μm/dec.[24] A planar graphene transistor design promises with a flexible distance sensor array in a direct-contact and active sensing fashion,[25] which has been proven to be low-power-consuming, highly efficient and simplified in fabrication process.[24,26] Hence, functional triboiontronic devices with broad choice of EDL materials are believed to have great potential in sophisticated and versatile electronics.

A proton conductor is a specific ionic-conducting material, which generally contains immobile polymer anions and mobile

Received: April 10, 2020
Accepted: June 22, 2020
Published: June 22, 2020

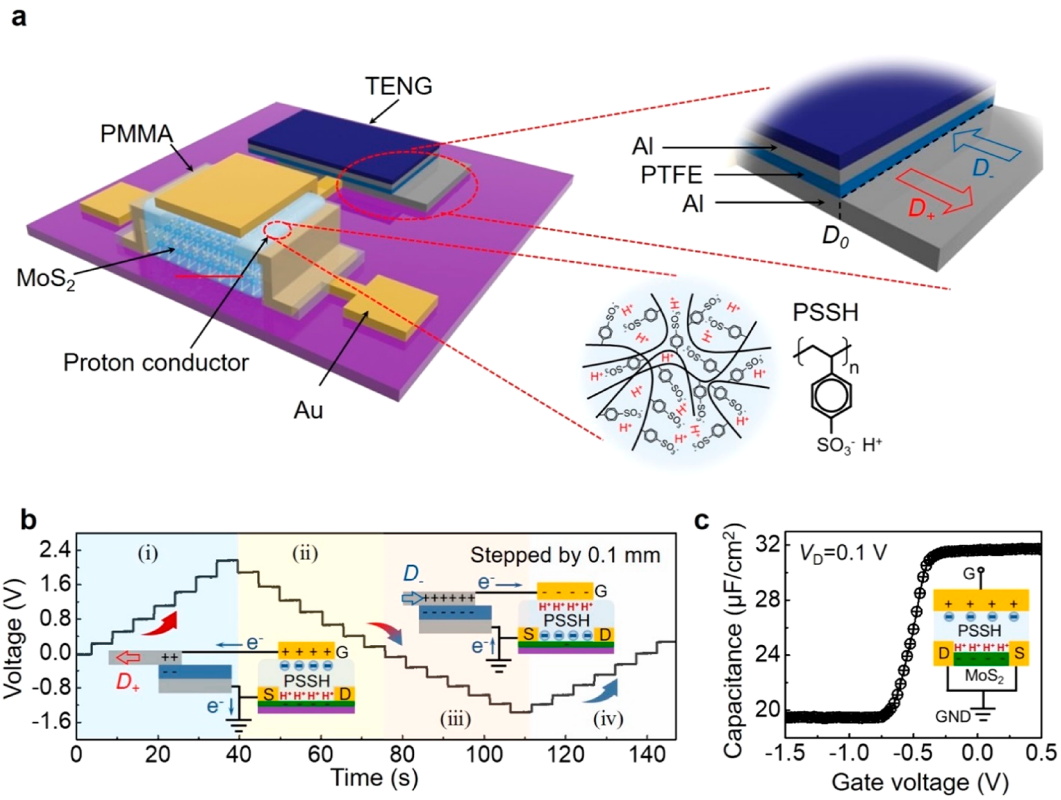

Figure 1. (a) Schematic illustration of the triboiontronic transistor *via* proton conductor. Top inset: enlarged structure of TENG component. Bottom inset: chemical structure of PSSH. (b) TENG output voltage (equivalent to the applied V_G) according to periodic displacement. (c) Capacitance of PSSH *versus* gate voltage based on PSSH gated MoS_2 transistor.

protons (H^+, the smallest and the most abundant ions).[27] It can realize a faster migration/polarization under electric field to form the EDL in the polyelectrolyte compared with other ions in larger size or volume.[13] Meanwhile, by elaborately utilizing the protons as the only mobile ions, it is more straightforward to control the conduction polarity in *n*-type semiconductor materials.[28] For the EDL formed at the interface with protons/electrons, the reduction of capacitor gap and the increased ion density at the interface can greatly enhance the EDL capacitance.[29] The protons also interact with the active material surface simply through electrostatic interactions without any chemical reaction/bonding, which is preferential for high performance electronics with excellent figure of merits and fast logic switching applications.[14,29] From the aspect of bioelectronics application, neuron connection, neutral information delivery, and synaptic plasticity are all modulated by protonic[27] or ionic fluxes.[30] Utilizing proton-conductor-gated EDL-FETs to directly mimic the neural functions has represented tremendous potential compared with traditional complementary metal oxide semiconductor (CMOS) neuromorphic circuits. The sophisticated combination of triboelectric modulation with protons migration may further achieve mechanical behavior derived multifunctional electronic devices.

Here, we demonstrate a versatile triboiontronic MoS_2 transistor *via* proton conductor, which utilizes triboelectric potential originated from mechanical displacement to modulate the electrical properties. The triboiontronic transistor is composed of a proton-conductor-gated MoS_2 transistor and a sliding-mode TENG. The triboelectric potential can drive protons to migrate fast and accumulate at the electrolyte/semiconductor interface to form EDL (with ultrahigh capacitance >10 $\mu F \cdot cm^{-2}$) and efficiently modulate the electrons transport in transistor channel. The triboiontronic MoS_2 transistor *via* proton conductor shows superior electrical properties, including high current on/off ratio over 10^6, low cutoff current (~0.04 pA), and steep switching properties (89 μm/dec). Pioneering low frequency current noise tests are introduced in tribotronic devices, which are highly desired for the mechanical behavior controlled electronics. From the drain−current noise spectra densities tests, it is demonstrated that no extra current noise interferes with the output currents during the mechanical operation process. The working mechanism of triboiontronic MoS_2 transistor *via* proton conductor is minutely explained based on the operation mode and energy band diagrams. Based on the proposed tribo-protonic gating transistor, we demonstrate the mechanical behavior derived tribotronic logic devices with good stability and high gain at 0.15 $V \cdot mm^{-1}$. Furthermore, an artificial sensory neuron system is demonstrated to decode the spatiotemporal input information on external mechanical displacements. A further simulation of mechanical behavior assisted visual imaging system is also carried out by using this artificial synapse. The multifunctional triboiontronic transistor *via* proton conductor demonstrates the reliable and effective triboelectric potential modulation on electronic transportation through protonic dielectrics. It is exceedingly desired for high performance mechanosensation, self-powered interactive interface, artificial intelligence, *etc.*

https://dx.doi.org/10.1021/acsnano.0c03030
ACS Nano XXXX, XXX, XXX−XXX

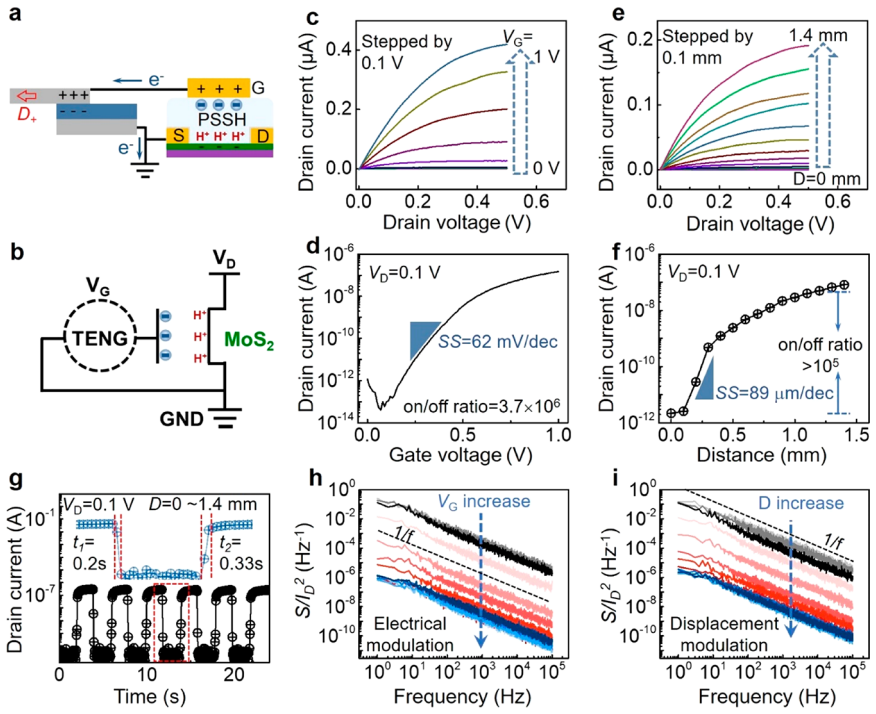

Figure 2. (a) Cross-sectional diagram and (b) equivalent circuit diagram of the PSSH gated triboiontronic transistor. (c) Typical output characteristics and (d) transfer characteristics of the PSSH gated MoS_2 transistor. (e) Tribotronic output characteristics and (f) corresponding transfer characteristics of the PSSH gated transistor modulated by TENG displacement. (g) Dynamic test of the triboiontronic transistor *via* proton conductor. The response time and decay time are 0.2 and 0.33 s, respectively. (h) Normalized drain−current noise spectra densities (S/I_D^2) of the PSSH gated transistor under different V_G conditions (from 0 to 1 V). The black dashed line is a standard 1/*f* noise guide. (i) Normalized drain−current noise spectra densities (S/I_D^2) of the triboiontronic transistor under different TENG displacements (from 0 to 1.4 mm). Both the normalized drain−current noise spectra densities in (h) and (i) are divided into three regions: cutoff region (black-series curves), subthreshold region (red-series curves), and on-state region (blue-series curves).

RESULTS AND DISCUSSION

Figure 1a shows a schematic illustration of the triboiontronic transistor *via* proton conductor, which includes a proton-conductor-gated MoS_2 transistor and a sliding mode TENG. In the triboiontronic transistor, MoS_2 is prepared by mechanical exfoliation and transferred on the SiO_2/Si substrate. Au source-drain electrodes are defined by e-beam lithography with subsequent thermal deposition process. Poly(styrenesulfonic) acid (PSSH, a kind of polyanionic polymer with chemical structure in the inset of Figure 1a) is selected as the dielectric layer, which is one of the representative proton conductors with protons as the only mobile cations and the fixed polymer chain as the counter polyanions. Before spin-coating the PSSH, it is necessary to pattern a thin layer of poly(methyl methacrylate) (PMMA, ~200 nm) on the source−drain electrodes to segregate them from the proton conductor and avoid the undesired leakage currents.[24] The Au gate electrode is thermally deposited on PSSH dielectrics to achieve the transistor component. The optical image of the specific device without PSSH is shown in Figure S1a. The thickness of mechanically exfoliated MoS_2 is estimated to be 2.7 nm by atomic force microscopy (AFM), corresponding to quadrilayer MoS_2. The Raman spectrum shows the vibration peak positions for the in-plane mode and the out-of-plane mode are at ~382 and 407 cm^{-1}, respectively, agreed well with the previously reported value for quadrilayer MoS_2 (Figure S1b).[31] In addition, the Raman spectrum of MoS_2 with PSSH has barely shifted, indicating no doping of protons to MoS_2.[32] In the photoluminescence spectrum, the peak position is ~680 nm, indicating the band gap of MoS_2 is ~1.82 eV (Figure S1c).[33]

The fabricated MoS_2 transistor is then integrated with a TENG in sliding mode (composed of polytetrafluoroethylene (PTFE) and Al friction layers) to realize the triboiontronic gating *via* the PSSH proton conductor. Upon the sliding action (or displacement) of TENG, the induced triboelectric potential dissociates the PSSH chains into protons and polyanions and drives protons to the PSSH/MoS_2 (or gate/PSSH) interface to form EDL with ultrahigh capacitance, which can efficiently modulate the Femi level of MoS_2 channel and the corresponding electronic transportation properties. Instead of applying gate voltage (V_G), the triboelectric potential induced by TENG displacement can be used to gate the transistor through the protonic solid-state electrolyte, *i.e.*, triboiontronic transistor *via* proton conductor. With Al friction layer connected to the transistor gate, we define an initial relative displacement between Al and PTFE friction layer as D_0 (inset of Figure 1a), at which the triboelectric potential is preset to be zero. The opposite-direction sliding (which will result in a decreased contact area between Al and PTFE) tends to drive the induced positive triboelectric charges transfer from Al film to the gate electrode. In other words, the opposite displacement will induce an equivalent positive V_G to the proton-conductor-gated MoS_2 FET, which is defined as positive displacement (D_+). To the contrary, the relative-direction sliding will result in an increased contact area with more triboelectric charges confined at the Al/PTFE interface, which can induce an equivalent negative V_G to the MoS_2 FET (defined as negative displacement, D_-). Figure 1b shows the

https://dx.doi.org/10.1021/acsnano.0c03030
ACS Nano XXXX, XXX, XXX−XXX

corresponding TENG output voltage (equivalent to the applied V_G) upon a periodic displacement (D, stepped at 0.1 mm). The curve can be divided into four regions: (i) With D increased from 0 to 0.7 mm (Al and PTFE contacts less), the output voltage increases step by step from 0 to 2.15 V due to more unbalanced electrostatic charges transfer to gate, which results in a positive triboelectric potential coupling to the MoS_2 FET. (ii) With D recovered step by step from 0.7 to 0 mm (to the initial D_0 position), the output voltage recovers from 2.15 to 0 V, exhibiting a similar variation in a reverse tend. (iii) With D further decreased from 0 to −0.7 mm (Al and PTFE contacts more), the output voltage decreases from 0 to −1.36 V. This is because the more positive triboelectric charges by electrostatic induction are confined at the Al/PTFE contact interface, resulting in a negative triboelectric potential coupling to the MoS_2 FET. (iv) When D gradually recovers to the preset initial position D_0, the negative TENG output vanishes step by step. The corresponding transferred charges and short-circuit current of the TENG component upon periodic displacement are represented in Figure S2 (the displacement speed is set to be 0.77 mm/s). All of the above results demonstrate that the TENG output performances vary steadily and synchronously with the TENG displacement, indicating the stable and excellent properties of the TENG component in the triboiontronic transistor.

The capacitive properties of the PSSH are investigated with a metal−insulator−metal (MIM) capacitor model (Au/PSSH/Au structure). Impedance spectroscopy is conducted to extract corresponding capacitive parameters by applying an AC voltage with frequency from 0.1 Hz to 0.1 MHz.[34] The frequency (f) dependent capacitance is illustrated in Figure S3a, which is 22 $\mu F \cdot cm^{-2}$ at a low frequency of 100 Hz and still higher than 1 $\mu F \cdot cm^{-2}$ at 10 kHz. The corresponding phase angle and Nyquist plot are also discussed in Figure S3b. To further characterize the capacitive properties of PSSH in proton-conductor-gated MoS_2 transistor, the $C-V$ measurement with metal−insulator-semiconductor (MIS) structure is also carried out. As shown in Figure 1c, the specific capacitance of the device increases from 20 to 32 $\mu F \cdot cm^{-2}$ with the gate voltage increased from −1.0 to 0.5 V, all of which are maintained in a high level during the operation of the proton-conductor-gated transistor. The effective capacitance evaluated from both MIM and MIS structures is >10 $\mu F \cdot cm^{-2}$, which is much higher than that achieved from conventional high-κ oxide dielectrics. This can be attributed to the fact that the protons (or polyanions) in PSSH are strongly accumulated at the PSSH/MoS_2 or PSSH/Au interfaces under an electric field to form the EDLs, which can be regarded as nanogap capacitors and possess ultrahigh capacitance. As the fundamental of triboiontronic transistor *via* proton conductor, the influence of triboelectric potential on proton migration and arrangement is also discussed in Figure S4.[35]

After confirming the effective triboelectric potential modulation and excellent dielectric properties of the PSSH, the electrical performances of triboiontronic MoS_2 transistor *via* proton conductor are fully investigated. Parts a and b of Figure 2 show the cross-sectional diagram of the PSSH-gated triboiontronic transistor and the equivalent circuit diagram. Under the TENG positive displacement D_+, the induced positive triboelectric potential will attract polyanions at the Au/PSSH interface and repel the protons to the PSSH/MoS_2 interface to form the EDLs. The basic electrical performances of the PSSH-gated MoS_2 transistor under applied V_G are first tested. Figure 2c displays the typical output performance of the PSSH-gated MoS_2 transistor measured at different V_G biases. The drain current (I_D) increases from 0.96 pA to 0.46 μA with V_G increased from 0 to 1 V at the drain voltage (V_D) of 0.5 V. It shows a linear dependence on V_D at lower V_D(0 to 0.1 V) and approaches saturation at higher V_D(>0.4 V). Figure 2d displays the transfer characteristics of the PSSH-gated MoS_2 transistor at V_D = 0.1 V. The device is turned on at a V_G close to 0 V, and I_D increases from 0.04 pA to 0.15 μA with increased V_G, achieving a high on/off ratio at 3.7×10^6. The field-effect mobility (μ) of the PSSH-gated MoS_2 transistor is ~0.25 $cm^2 \cdot V^{-1} \cdot s^{-1}$ (Figure S5a). The subthreshold swing (SS) is derived to be 62 mV/dec (Figure S5b, close to the theoretical limit value of 60 mV/dec), which may be attributed to the ultrahigh capacitance of the PSSH protonic electrolyte gate dielectrics greatly decreases the operating V_G (<1 V).

For the MoS_2 transistor under triboelectric potential protonic gating, the tribotronic output performance is shown in Figure 2e. Relying on the triboelectric potential induced by TENG displacement D, the I_D increases with the increased D and exhibits a similar variation trend with the output performance in Figure 2c. The corresponding tribotronic transfer characteristics (I_D *vs* D) extracted from the output characteristics are shown in Figure 2f. I_D increases from 2.2 pA to 81.2 nA with D changed from 0 to 1.4 mm at V_D = 0.1 V. The TENG displacement of 1.4 mm is estimated to be equivalent to a V_G of 1 V. The excellent electrical performances of the triboiontronic transistor *via* proton conductor indicate the triboelectric potential originated from the TENG displacement is effective in gating the MoS_2 transistor through protonic electrolyte. The current on/off ratio under TENG displacement (D from 0 to 1.4 mm) is ~10^5, which can be further enhanced by applying available larger range of D. Analogy to the characterization of electrical g_m and SS, corresponding tribotronic transconductance (g_t) and tribotronic subthreshold swing (SS_t) can be derived by replacing the V_G with D in relevant formulas, which are estimated to be ~0.16 μA/mm and 89 μm/dec, respectively (Figure S5d,e). The tribotronic subthreshold swing is much better than the counterparts of tribotronic FET with traditional SiO_2 dielectrics (SS_t = 4.6 mm/dec)[36] and comparable with that of ion-gel-gated tribotronic transistor (SS_t = 20 μm/dec).[24] A real-time dynamic test of the triboiontronic transistor is also conducted in Figure 2g. Thanks to the ultralow gate leakage current (~ pA level), I_D varies accordingly under the periodic TENG displacement (direct change from 0 to 1.4 mm), realizing high on/off ratio (~10^6) with stable on/off-state currents. The forward and backward response time during the dynamic test is extracted to be 0.2 and 0.33 s, respectively. The relatively slower backward response time (or decay time) is preferential for the potential application of the triboiontonic transistor *via* proton conductor as an artificial synaptic device.

In general, the channel current noises commonly exist in FET device and appear as $1/f$ noise at low frequency,[37,38] which is resulted from the charge trapping and detrapping effect at the interface of channel and dielectric layer. In this work, we introduce current noise test to the tribotronic transistor to probe whether the mechanical displacements of the TENG component can introduce extra current noise during the device operation. The drain−current noise spectra densities (S) of the MoS_2 transistor modulated by different V_Gs and TENG displacements are measured at V_D = 0.1 V, respectively. The current noises in both cases show the

https://dx.doi.org/10.1021/acsnano.0c03030
ACS Nano XXXX, XXX, XXX−XXX

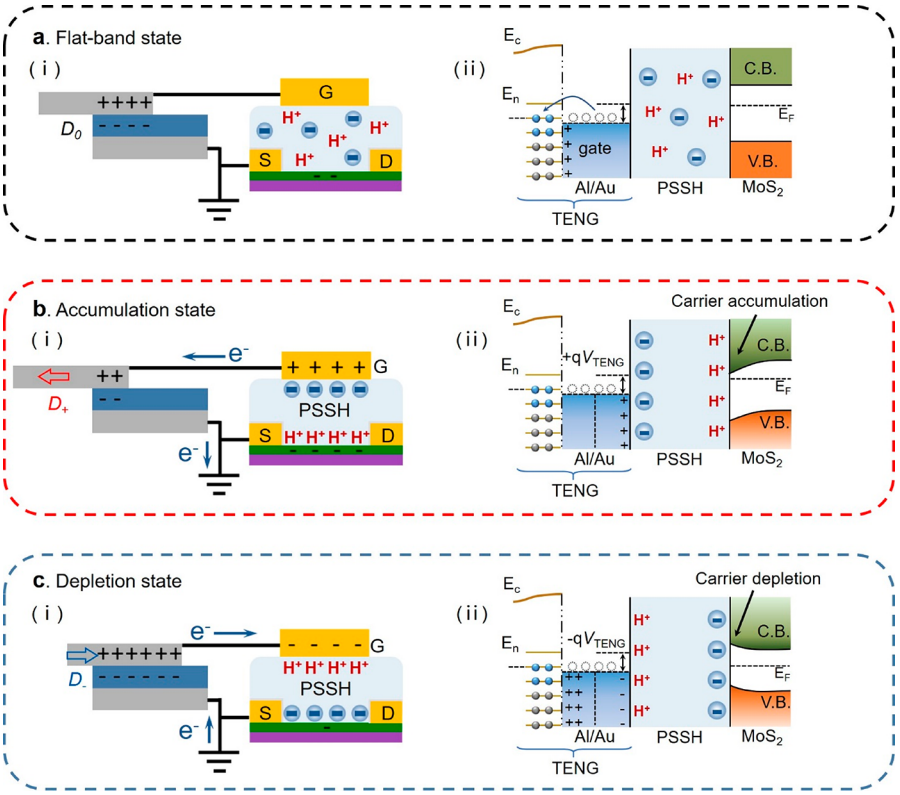

Figure 3. Working mechanism of the PSSH gated triboiontronic transistor, explained by operation diagram and energy band diagram, respectively. (a) Flat-band state with a preset position of the TENG component. (b) Accumulation state upon positive displacement (D_+), equivalent to applying positive V_G. (c) Depletion state upon negative displacement (D_-), equivalent to applying negative V_G.

increment trend with increased V_G and D, mainly dominated by the I_D value (Figure S5c and S 5f). The normalized drain–current noise spectra densities (S/I_D^2) are illustrated in Figure 2h and 2i. The current noises under the modulation of V_G and D both show decrement trends according to the increased V_G and D, even at the most sensitive subthreshold region (red series curves). The low-frequency noise results for the MoS_2 transistor under both electrical and mechanical modulations exhibit the similar variation range and obey the standard $1/f$ noise theory,[39,40] which is originated from the fluctuations of current. That is, the I_Ds of the MoS_2 transistors modulated by both V_G and D have not been disturbed by thermal noise or others. Both the excellent electrical properties and standard $1/f$ current noises indicate that tribotronic gating is a reliable way for a stable transistor operation. The in-depth comprehension of triboelectric potential modulation on the EDL transistors by current noise analysis is of great significance for the theoretical study on triboiontronic device and its practical applications.

The working mechanism of the triboiontronic transistor *via* proton conductor at three operation states (*i.e.*, flat-band state, accumulation, and depletion states) are elaborately discussed in regard to the triboelectrification-induced charge transfer, proton/polyanion distribution, and corresponding energy band diagrams (Figure 3). The triboiontronic transistor *via* proton conductor is constructed with an Al friction layer connected to the transistor gate and the other electrode connected to the ground. At the beginning (flat-band state), Al and PTFE friction layers of the TENG component are preset at an initial relative position to achieve the zero triboelectric potential. There are no triboelectric charges transferred to the gate electrode. In this state, no triboelectric potential is applied to the MoS_2 transistor through the protonic PSSH dielectrics. The protons and polyanions in PSSH are distributed randomly and the charge carrier density in MoS_2 channel maintains the pristine value (Figure 3a(i)). From the aspect of the energy band diagram, partial electrons in Al film transfer to the PTFE film at their first contact due to different electronegativity, which are balanced by the counter positive triboelectric charges at the contact interface and results in a neutralized state of the TENG. As no electric field is imposed on MoS_2 channel, its conduction band and valence band both keep in the flat-band state (Figure 3a(ii)). When D_+ (opposite displacement between Al and PTFE) is applied to the TENG, more induced positive triboelectric charges in Al film are lack of restriction and transferred to the gate electrode of MoS_2 transistor, equivalent to applying a positive V_G. The transferred positive charges repel the protons to the PSSH/MoS_2 interface, which can induce the increased electrons density in MoS_2 channel, *i.e.*, the accumulation state (Figure 3b(i)). The relevant energy band diagram is shown in Figure 3b(ii), D_+ induces a positive triboelectric potential coupling to the MoS_2 transistor, resulting in the accumulation of protons at PSSH/MoS_2 interface to induce more electrons in MoS_2 channel and bend the MoS_2 energy band downward. When D_- (relative displacement between Al and PTFE) is applied to the TENG, more positive triboelectric charges are confined at the Al/PEFE interface and lead to more counter electrons transfer to the transistor gate, equivalent to applying a negative V_G. The transferred electrons attract most protons to the Au/PSSH interface, thereby decreasing the electrons density in MoS_2 channel (*i.e.*, the depletion state, Figure 3c(i)). The relevant energy band diagram is shown in Figure 3c(ii), D_-

https://dx.doi.org/10.1021/acsnano.0c03030
ACS Nano XXXX, XXX, XXX−XXX

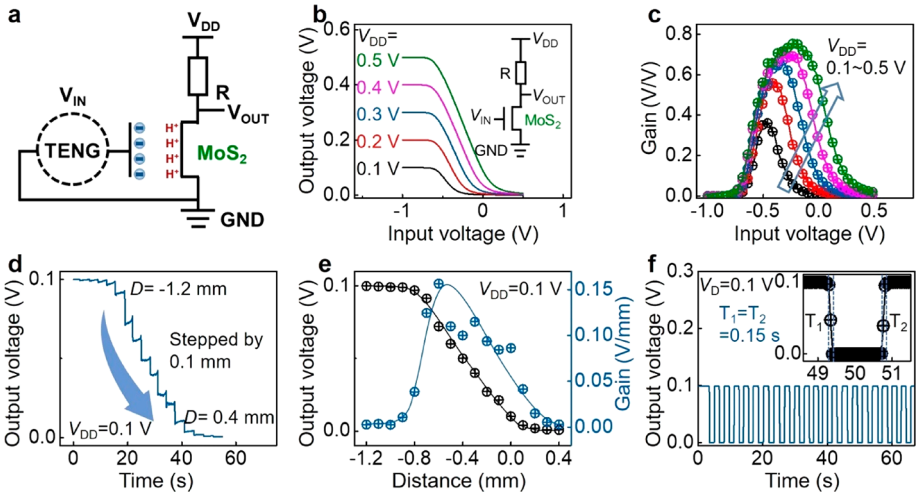

Figure 4. (a) Circuit diagram of the triboiontronic logic device *via* proton conductor. (b) Typical voltage transfer characteristics and (c) corresponding gain values of the PSSH gated transistor under V_{DD} = 0.1 to 0.5 V stepped by 0.1 V. (d) Real-time test of the triboiontronic inverter with TENG displacement decreased from 0.4 to −1.2 mm. (e) Extracted voltage transfer characteristics and corresponding gain value of the triboiontronic inverter under *D* increased from −1.2 to 0.4 mm at V_{DD} = 0.1 V. (f) Dynamic cycle test of the triboiontronic inverter. The response time and decay time are 0.15 s.

induces a negative triboelectric potential coupling to the MoS_2 transistor, resulting in the accumulation of polyanions at PSSH/MoS_2 interface to decrease the electrons density in MoS_2 channel and bend the MoS_2 energy band upward. Upon the triboelectric potential gating, the charge carrier density and corresponding energy band can be effectively modulated *via* protonic dielectrics.

The stable electrical properties, high current on/off ratio and paired resistance of the triboiontronic transistor *via* proton conductor meet the requirements for logic gate. On this basis, we demonstrate the application of triboiontronic device as a logic inverter with a load-resistor (10 MΩ) connected in series (electrical circuit diagram in Figure 4a). Typical voltage transfer curves of the inverter under applied V_G are characterized in Figure 4b. Under the superposition effect of the applied driving voltage (V_{DD} from 0.1 to 0.5 V), the voltage drop on the series resistor varies according to the resistance change of MoS_2 transistor, leading to an inverted signal between the input (V_{IN}) and output voltage (V_{OUT}). All of the V_{OUT}s coincide well with the applied V_{DD}s (corresponding to the output logic "1") at V_{IN} of −1.0 V (corresponding to the input logic "0") and decrease to nearly 0 V (corresponding to the output logic "0") at V_{IN} of 0.5 V (corresponding to the input logic "1"), exhibiting a basic logic gate function. The corresponding voltage gains (G_V, expressed as $G_V = -dV_{OUT}/dV_{IN}$) are extracted in Figure 4c. The maximum gain value under different V_{DD}s increases from 0.37 to 0.75 with V_{DD} increasing from 0.1 to 0.5 V, and the corresponding sharp signal inversion position shifts from V_{IN} = −0.46 V to V_{IN} = −0.23 V. These results indicate that the PSSH-gated MoS_2 inverter is qualified to realize a normative 180° phase reversal from input to output. For the triboiontronic inverter *via* proton conductor, the TENG displacement replaces the applied V_G as the input signal. As shown in Figure 4d, upon *D* varying from −1.2 to 0.4 mm stepped by 0.1 mm at V_{DD} = 0.1 V, the V_{OUT} realizes a complete inversion from 0.1 V (output logic "1") to 0 V (output logic "0"). The average V_{OUT} at each step is extracted and plotted in Figure 4e, which shows a similar variation trend with the voltage transfer curves in Figure 4b. The corresponding tribotronic gain (G_T) to evaluate the transition status of logic states can be derived from equation: $G_T = -dV_{OUT}/dD$, which reaches the maximum value of 0.16 V·mm^{-1} at the logic switching point of −0.6 mm. A real-time dynamic test is also conducted to the triboiontronic logic device with over 20 cycles (Figure 4f). Every cycle shows a stable and normative logic separation with response time (T_1) and decay time (T_2) at ∼0.15 s. The corresponding inverter current also varies stably upon the periodic displacement as shown in Figure S6. Excellent and stable inverter properties indicate the triboiontronic transistor *via* proton conductor is ready to be used in more complex logic gates modulated by mechanical actions.

Relying on the mechanical displacement derived proton migration and its intrinsic relaxation behavior (Figure S7), the triboiontronic transistor *via* proton conductor is further demonstrated as an artificial sensory neuron system. As shown in Figure 5a, the TENG component can mimic the mechanoreceptor to deliver the presynaptic signals, while the PSSH-gated transistor can work as a postsynaptic device to implement corresponding order by postsynaptic current (PSC).[41] The pulse mechanical displacement input with spatiotemporal information can be converted into spike triboelectric signal, delivered to the PSSH-gated synaptic transistor, and reflected in the PSC. Typical short-term plasticity behaviors of a neuron synapse, including potentiation, inhibition and paired pulse facilitation (PPF) modulated by mechanical displacement are demonstrated in the triboiontronic synaptic device *via* proton conductor. Parts b and c of Figure 5 display the potentiation of PSCs triggered by two different groups of *D* pulse patterns including either spatial or temporal information, respectively. With the *D* pulse increased from 0.2 to 1.4 mm at a duration time of 0.2 s (*i.e.*, spatial pattern),[20,42] the corresponding PSC increases from 5.7 to 34.2 nA (Figure 5b). The larger *D* pulse produces a larger triboelectric potential and induces more protons accumulation at the PSSH/MoS_2 interface to modulate the Fermi level of MoS_2 channel, resulting in higher PSC. Figure 5c displays the PSCs triggered by *D* pulses with different duration time (*i.e.*, temporal patterns).[42] With *D* pulse duration increased from 0.27 to 0.85 s at a constant displacement of 0.2 mm, the PSC

https://dx.doi.org/10.1021/acsnano.0c03030
ACS Nano XXXX, XXX, XXX−XXX

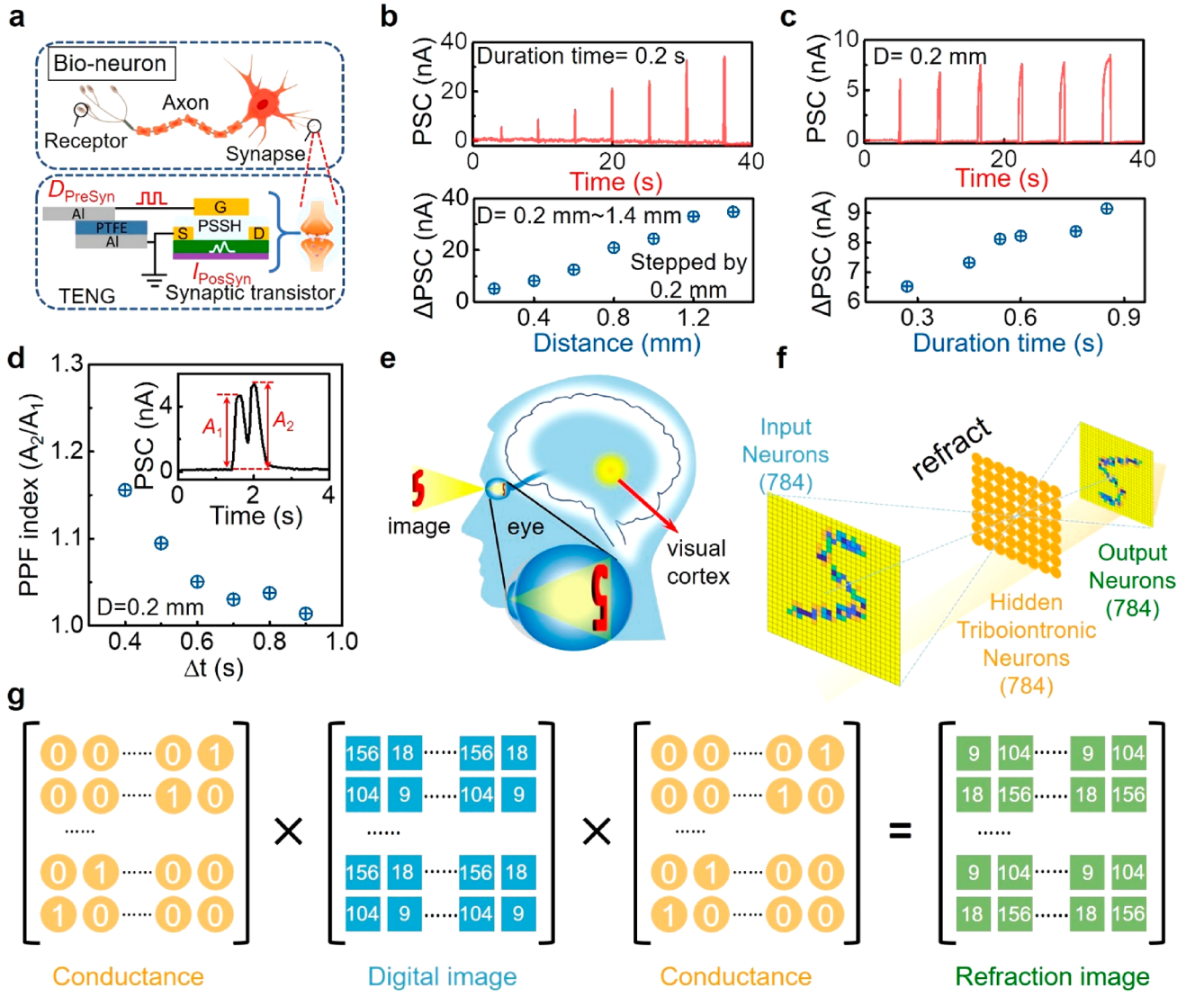

Figure 5. Artificial synaptic simulation based on the triboiontronic transistor *via* proton conductor. (a) Schematic illustration of a bioneuron and corresponding triboiontronic sensory neuron. (b) TENG displacement dependent PSCs as a function of time (above) and corresponding ΔPSC values (below), where V_D = 0.1 V and the duration time of *D* pulse is 0.2 s. (c) Duration of time-dependent PSCs as a function of time (above) and corresponding ΔPSC values (below), where V_D = 0.1 V and *D* = 0.2 mm. (d) PPF index, defined as the ratio of A_2/A_1, as a function of interspike interval (Δ*t*). Inset is a typical PSC response activated by a pair of D pulse (*D* = 0.2 mm and Δ*t* = 0.4 s). (e) Illustration of the visual imaging system. (f) Simulation of image inversion in visual imaging by building matrix multiplication accelerator with the triboiontronic artificial synaptic transistor. (g) Working mechanism of the matrix multiplication accelerator.

increases from 6.5 to 9.0 nA. The longer duration of the *D* pulse gives enough time for the proton to be fully accumulated at the PSSH/MoS_2 interface, which can more effectively enhance the electrons transport in MoS_2 channel and lead to higher PSC. To further characterize the synaptic plasticity behavior, the PPF triggered by mechanical displacement is investigated. Inset of Figure 5d shows the typical PPF behavior with PSC triggered by a pair of presynaptic *D* pulses (amplitude at 0.2 mm, duration of 0.2 s) with pulses interval (Δ*t*) at 0.4 s. The PSC peak (5.2 nA) triggered by the second *D* pulse is larger than that (4.6 nA) triggered by the first pulse. This is attributed to that part of the accumulated protons triggered by the first *D* pulse cannot diffuse back to the initial random state when the second *D* pulse arrives, which induces more accumulated protons to modulate the electrons density in MoS_2 channel and results in the second higher consecutive PSC. Notably, the PPF behavior almost disappears when the interval time of *D* pulses is larger than 0.9 s, which is not contradictory with the stable dynamic test of the triboiontronic transistor with displacement interval at 2 s as demonstrated in Figure 2g. A series of paired *D* pulses (amplitude at 0.2 mm, duration of 0.2 s) with different intervals are further applied on the tribotronic synaptic device (Figure S8a). The PPF index defined as A_2/A_1 (where A_1 and A_2 are the PSC amplitudes of the first and second spikes, respectively) decreases from 1.16 to 1.01 with the increased Δ*t* from 0.4 to 0.9 s, consistent with the relaxation behavior of protons migration. The potentiation and inhibitory plasticity of the artificial synapse triggered by multiple consecutive *D* pulses (pulse number is 50) is also investigated (Figure S8b–d), exhibiting relevant increment or decrement in the PSC peak values according to the *D* pulse numbers. The demonstrated potentiation/inhibitory, synaptic plasticity, and PPF in the triboiontronic transistor *via* proton conductor are highly analogic to the behavior of biosynapse.

https://dx.doi.org/10.1021/acsnano.0c03030
ACS Nano XXXX, XXX, XXX−XXX

As the synaptic weight (*i.e.*, the channel conductance) of PSSH-gated transistor can be significantly modulated by the mechanical displacement, we can utilize the triboiontronic device to simulate a mechanical behavior assisted visual imaging system which realizes the reversion transform of an object image through a multilayer neuron simulation network (Figure S8e). As is known, the image of an object in retina is centrosymmetric to the real object (right to left and upside to downside). The object information is transformed into nerve signals, which are subsequently transferred to the visual cortex, analyzed, and recognized as a reversed visual image (Figure 5e). Here, the input digital information on number "5" from 784 neurons are delivered to the mediate neural layer, processed by the hidden neural layer (simulated by the triboiontronic synaptic devices), and inverted to obtain the reversed digital information on number "5" from the output neurons (Figure 5f). The working mechanism is sketched in Figure 5g with matrix multiplication accelerator. This mechanical displacement modulated synaptic device may be helpful for the touch assisted braille recognition system.

CONCLUSION

Based on the triboelectric potential modulation on the electrical properties *via* protons migration/arrangement, a versatile triboiontronic MoS_2 transistor has been demonstrated. Its working mechanism is minutely explained based on the operation mode and energy band diagrams. Superior electrical properties have been achieved, such as high current on/off ratio ($>10^6$), low cutoff current (~0.04 pA), and steep switching properties (89 μm·dec^{-1}). Low frequency current noise tests demonstrate that no extra current noise interferes with the transistor output performance during the mechanical displacement gating process. The triboiontronic MoS_2 transistor *via* proton conductor has been used as a highly stable mechanical behavior derived logic devices and an artificial sensory neuron system to simulate a mechanical behavior assisted visual imaging system. The versatile triboiontronic transistor *via* proton conductor offers an effective technique to multifunctional and low-power-consuming electronic devices, such as human–machine interaction, electronic skin, and intelligent wearable devices, *etc.*

METHODS

Materials and devices preparation: *N*-type doped Si wafer with 300 nm SiO_2 layer was served as the substrate. Few-layer MoS_2 flakes were prepared through mechanically exfoliation method from the purchased natural bulk MoS_2. Then source-drain electrodes (Cr/Au, 5/40 nm) were patterned on MoS_2 flake through standard electron beam lithography (EBL) and thermal evaporation deposition process. Next, a 200 nm PMMA was spin-coated on top to protect these electrodes, and a second EBL process was conducted to expose the channel areas. After that, 9 wt % PSSH water solution was spin-coated onto the substrate at 3000 rpm for 60 s, followed with a thermal annealing process at 110 °C for 60 s. Finally, the top gate electrodes were deposited through a shadow mask. TENG composed of an Al/PTFE/Al structure was integrated on the extended transistor gate electrode.

PSSH MIM capacitor: the Cr/Au metal layer was first prepared on the SiO_2/Si substrate by thermal evaporation process. Then aqueous PSSH solution (9 wt %) was spin-coated onto the surface of the Au electrode with the same parameter as above. Finally, the top Au electrodes were thermally deposited through a shadow mask to achieve the MIM mode capacitor.

Performance characterization: The surface topography and thickness of few-layer MoS_2 was characterized by AFM. The Raman and photoluminescence (PL) characteristics of MoS_2 were measured by HORIBA/labRAM evolution spectrograph with emission laser at 532 nm. The displacements of TENG were precisely controlled by a motorized positioning system, and the output properties were measured by a Keithley 6514 electrometer. The capacitance of PSSH was measured with an electrical workstation (CHI 660E). The electrical performance of the transistor was characterized with a semiconductor device analyzer (Agilent B1500A) with a probe station. The drain–current noise spectra densities were measured with a noise measurement system (PDA NC300L, 100 kHz bandwidth). During the test, the device and the TENG should be well screened to protect the test system from the disturbance of surrounding electrostatic charges. All of these tests were carried out at room temperature and ambient environment.

ASSOCIATED CONTENT

Supporting Information

The Supporting Information is available free of charge at https://pubs.acs.org/doi/10.1021/acsnano.0c03030.

Characterization of the mechanical exfoliated few-layer MoS_2; electrical characterization of the sliding-mode TENG component; impedance analysis of PSSH capacitor with MIM structure; discussion of triboelectric potential influence on protons migration and arrangement in PSSH; electrical performances of PSSH-gated transistor and corresponding tribotronic properties; current performances of the tribotronic logic inverter *via* proton conductor; mechanism of synaptic behavior of the PSSH-gated triboiontronic transistor; simulation of short-term synaptic plasticity behaviors in the triboiontronic transistor (PDF)

AUTHOR INFORMATION

Corresponding Authors

Qijun Sun – *Beijing Institute of Nanoenergy and Nanosystems, Chinese Academy of Sciences, Beijing 100083, China; School of Nanoscience and Technology, University of Chinese Academy of Sciences, Beijing 100049, China; Center on Nanoenergy Research, School of Physical Science and Technology, Guangxi University, Nanning 530004, China;* orcid.org/0000-0003-2130-7389; Email: sunqijun@binn.cas.cn

Zhong Lin Wang – *Beijing Institute of Nanoenergy and Nanosystems, Chinese Academy of Sciences, Beijing 100083, China; School of Nanoscience and Technology, University of Chinese Academy of Sciences, Beijing 100049, China; School of Materials Science and Engineering, Georgia Institute of Technology, Atlanta, Georgia 30332-0245, United States;* Email: zhong.wang@mse.gatech.edu

Authors

Xixi Yang – *Beijing Institute of Nanoenergy and Nanosystems, Chinese Academy of Sciences, Beijing 100083, China; School of Nanoscience and Technology, University of Chinese Academy of Sciences, Beijing 100049, China; CAS Center for Excellence in Nanoscience, National Center for Nanoscience and Technology (NCNST), Beijing 100190, P. R. China*

Jing Han – *Beijing Institute of Nanoenergy and Nanosystems, Chinese Academy of Sciences, Beijing 100083, China; School of Nanoscience and Technology, University of Chinese Academy of Sciences, Beijing 100049, China*

Jinran Yu – *Beijing Institute of Nanoenergy and Nanosystems, Chinese Academy of Sciences, Beijing 100083, China; School of Nanoscience and Technology, University of Chinese Academy of Sciences, Beijing 100049, China*

https://dx.doi.org/10.1021/acsnano.0c03030
ACS Nano XXXX, XXX, XXX–XXX

Youhui Chen − *Beijing Institute of Nanoenergy and Nanosystems, Chinese Academy of Sciences, Beijing 100083, China; School of Nanoscience and Technology, University of Chinese Academy of Sciences, Beijing 100049, China*

Huai Zhang − *Beijing Institute of Nanoenergy and Nanosystems, Chinese Academy of Sciences, Beijing 100083, China; School of Nanoscience and Technology, University of Chinese Academy of Sciences, Beijing 100049, China*

Mei Ding − *College of Materials Science and Engineering, Changsha University of Science & Technology, Changsha 410114, China*

Chuankun Jia − *College of Materials Science and Engineering, Changsha University of Science & Technology, Changsha 410114, China*

Jia Sun − *School of Physics and Electronics, Central South University, Changsha 410083, China;* orcid.org/0000-0003-4423-8128

Complete contact information is available at: https://pubs.acs.org/10.1021/acsnano.0c03030

Author Contributions

[Δ]X.Y., J.H., and J.Y. contributed equally.

Notes

The authors declare no competing financial interest.

ACKNOWLEDGMENTS

This work is finacially supported by the National Key Research and Development Program of China (2016YFA0202703, 2016YFA0202704), National Natural Science Foundation of China (51605034, 51711540300), CAS Pioneer Hundred Talents Program, Beijing Nova Program (Z191100001119047), and the State Key Laboratory of Precision Measuring Technology and Instruments (Tianjin University).

REFERENCES

(1) Qin, S.; Zhang, Q.; Yang, X.; Liu, M.; Sun, Q.; Wang, Z. L. Hybrid Piezo/Triboelectric-Driven Self-Charging Electrochromic Supercapacitor Power Package. *Adv. Energy. Mater.* **2018**, *8*, 1800069.

(2) Matyba, P.; Maturova, K.; Kemerink, M.; Robinson, N. D.; Edman, L. The Dynamic Organic *p-n* Junction. *Nat. Mater.* **2009**, *8*, 672−676.

(3) Zeng, S. W.; Huang, Z.; Lv, W. M.; Bao, N. N.; Gopinadhan, K.; Jian, L. K.; Herng, T. S.; Liu, Z. Q.; Zhao, Y. L.; Li, C. J. Two-Dimensional Superconductor-Insulator Quantum Phase Transitions in an Electron-Doped Cuprate. *Phys. Rev. B: Condens. Matter Mater. Phys.* **2015**, *92*, 020503.1−020503.7.

(4) Zhang, Y.; Ye, J.; Matsuhashi, Y.; Iwasa, Y. Ambipolar MoS_2 Thin Flake Transistors. *Nano Lett.* **2012**, *12*, 1136−1140.

(5) Yuan, H.; Shimotani, H.; Tsukazaki, A.; Ohtomo, A.; Kawasaki, M.; Iwasa, Y. High-Density Carrier Accumulation in ZnO Field-Effect Transistors Gated by Electric Double Layers of Ionic Liquids. *Adv. Funct. Mater.* **2009**, *19*, 1046−1053.

(6) Qian, C.; Sun, J.; Kong, L.-A.; Fu, Y.; Chen, Y.; Wang, J.; Wang, S.; Xie, H.; Huang, H.; Yang, J.; Gao, Y. Multilevel Nonvolatile Organic Photomemory Based on Vanadyl-Phthalocyanine/Para-Sexiphenyl Heterojunctions. *ACS Photonics* **2017**, *4*, 2573−2579.

(7) Lei, Z.; Wu, P. A Supramolecular Biomimetic Skin Combining a Wide Spectrum of Mechanical Properties and Multiple Sensory Capabilities. *Nat. Commun.* **2018**, *9*, 1134.

(8) Chortos, A.; Liu, J.; Bao, Z. Pursuing Prosthetic Electronic Skin. *Nat. Mater.* **2016**, *15*, 937−950.

(9) Sun, J. Y.; Keplinger, C.; Whitesides, M. C.; Suo, Z. Ionic Skin. *Adv. Mater.* **2014**, *26*, 7608−7614.

(10) Larson, C. Highly Stretchable Electroluminescent Skin for Optical Signaling and Tactile Sensing. *Science* **2016**, *351*, 1071−1074.

(11) Lin, S.; Yuk, H.; Zhang, T.; Parada, G. A.; Koo, H.; Yu, C.; Zhao, X. Stretchable Hydrogel Electronics and Devices. *Adv. Mater.* **2016**, *28*, 4497−4505.

(12) Miao, X.; Tongay, S.; Petterson, M. K.; Berke, K.; Rinzler, A. G.; Appleton, B. R.; Hebard, A. F. High Efficiency Graphene Solar Cells by Chemical Doping. *Nano Lett.* **2012**, *12*, 2745−2750.

(13) Bisri, S. Z.; Shimizu, S.; Nakano, M.; Iwasa, Y. Endeavor of Iontronics: From Fundamentals to Applications of Ion-Controlled Electronics. *Adv. Mater.* **2017**, *29*, 1607054.

(14) Choi, Y.; Kim, H.; Yang, J.; Shin, S. W.; Um, S. H.; Lee, S.; Kang, M. S.; Cho, J. H. Proton-Conductor-Gated MoS_2 Transistors with Room Temperature Electron Mobility of > 100 $cm^2\ V^{-1}\ s^{-1}$. *Chem. Mater.* **2018**, *30*, 4527−4535.

(15) Ueno, K.; Nakamura, S.; Shimotani, H.; Ohtomo, A.; Kimura, N.; Nojima, T.; Aoki, H.; Iwasa, Y.; Kawasaki, M. Electric-Field-Induced Superconductivity in an Insulator. *Nat. Mater.* **2008**, *7*, 855−858.

(16) Costanzo, D.; Jo, S.; Berger, H.; Morpurgo, A. F. Gate-Induced Superconductivity in Atomically Thin MoS_2 Crystals. *Nat. Nanotechnol.* **2016**, *11*, 339−344.

(17) Shimizu, S.; Bahramy, M. S.; Iizuka, T.; Ono, S.; Miwa, K.; Tokura, Y.; Iwasa, Y. Enhanced Thermopower in ZnO Two-Dimensional Electron Gas. *Proc. Natl. Acad. Sci. U. S. A.* **2016**, *113*, 6438−6443.

(18) Wang, J.; Chen, Y.; Kong, L.-A.; Fu, Y.; Gao, Y.; Sun, J. Deep-Ultraviolet-Triggered Neuromorphic Functions in In-Zn-O Phototransistors. *Appl. Phys. Lett.* **2018**, *113*, 151101.

(19) Sun, J.; Fu, Y.; Wan, Q. Organic Synaptic Devices for Neuromorphic Systems. *J. Phys. D: Appl. Phys.* **2018**, *51*, 314004.

(20) Chen, Y.; Gao, G.; Zhao, J.; Zhang, H.; Yu, J.; Yang, X.; Zhang, Q.; Zhang, W.; Xu, S.; Sun, J.; Meng, Y.; Sun, Q. Piezotronic Graphene Artificial Sensory Synapse. *Adv. Funct. Mater.* **2019**, *29*, 1900959.

(21) Wang, Z. L. On Maxwell's Displacement Current for Energy and Sensors: The Origin of Nanogenerators. *Mater. Today* **2017**, *20*, 74−82.

(22) Wang, Z. L. On the First Principle Theory of Nanogenerators from Maxwell's Equations. *Nano Energy* **2020**, *68*, 104272.

(23) Liu, Y.; Zhong, J.; Li, E.; Yang, H.; Wang, X.; Lai, D.; Chen, H.; Guo, T. Self-Powered Artificial Synapses Actuated by Triboelectric Nanogenerator. *Nano Energy* **2019**, *60*, 377−384.

(24) Gao, G.; Yu, J.; Yang, X.; Pang, Y.; Zhao, J.; Pan, C.; Sun, Q.; Wang, Z. L. Triboiontronic Transistor of MoS_2. *Adv. Mater.* **2019**, *31*, 1806905.

(25) Meng, Y.; Zhao, J.; Yang, X.; Zhao, C.; Qin, S.; Cho, J. H.; Zhang, C.; Sun, Q.; Wang, Z. L. Mechanosensation-Active Matrix Based on Direct-Contact Tribotronic Planar Graphene Transistor Array. *ACS Nano* **2018**, *12*, 9381−9389.

(26) Zhang, H.; Yu, J.; Yang, X.; Gao, G.; Qin, S.; Sun, J.; Ding, M.; Jia, C.; Sun, Q.; Wang, Z. L. Ion Gel Capacitively-Coupled Tribotronic Gating for Multi-Parameter Distance Sensing. *ACS Nano* **2020**, *14*, 3461−3468.

(27) Kong, L.-A.; Sun, J.; Qian, C.; Gou, G.; He, Y.; Yang, J.; Gao, Y. Ion-Gel Gated Field-Effect Transistors with Solution-Processed Oxide Semiconductors for Bioinspired Artificial Synapses. *Org. Electron.* **2016**, *39*, 64−70.

(28) Larsson, O.; Said, E.; Berggren, M.; Crispin, X. Insulator Polarization Mechanisms in Polyelectrolyte-Gated Organic Field-Effect Transistors. *Adv. Funct. Mater.* **2009**, *19*, 3334−3341.

(29) Kim, H.; Kim, B. J.; Sun, Q.; Kang, M. S.; Cho, J. H. Graphene Transistors Gated by Salted Proton Conductor. *Adv. Electron. Mater.* **2016**, *2*, 1600122.

(30) Kong, L.-A.; Sun, J.; Qian, C.; Wang, C.; Yang, J.; Gao, Y. Spatially-Correlated Neuron Transistors with Ion-Gel Gating for Brain-Inspired Applications. *Org. Electron.* **2017**, *44*, 25−31.

(31) Li, H.; Zhang, Q.; Yap, C. C. R.; Tay, B. K.; Edwin, T. H. T.; Olivier, A.; Baillargeat, D. From Bulk to Monolayer MoS_2: Evolution of Raman Scattering. *Adv. Funct. Mater.* **2012**, *22*, 1385−1390.
(32) Zhao, J.; Li, N.; Yu, H.; Wei, Z.; Liao, M.; Chen, P.; Wang, S.; Shi, D.; Sun, Q.; Zhang, G. Highly Sensitive MoS_2 Humidity Sensors Array for Noncontact Sensation. *Adv. Mater.* **2017**, *29*, 1702076.
(33) Wang, Q. H.; Kalantar-Zadeh, K.; Kis, A.; Coleman, J. N.; Strano, M. S. Electronics and Optoelectronics of Two-Dimensional Transition Metal Dichalcogenides. *Nat. Nanotechnol.* **2012**, *7*, 699−712.
(34) Yang, X.; Hu, G.; Gao, G.; Chen, X.; Sun, J.; Wan, B.; Zhang, Q.; Qin, S.; Zhang, W.; Pan, C.; Sun, Q.; Wang, Z. L. Coupled Ion-Gel Channel-Width Gating and Piezotronic Interface Gating in ZnO Nanowire Devices. *Adv. Funct. Mater.* **2019**, *29*, 1807837.
(35) Braga, D.; Gutierrez Lezama, I.; Berger, H.; Morpurgo, A. F. Quantitative Determination of the Band Gap of WS_2 with Ambipolar Ionic Liquid-Gated Transistors. *Nano Lett.* **2012**, *12*, 5218−5223.
(36) Gao, G.; Wan, B.; Liu, X.; Sun, Q.; Yang, X.; Wang, L.; Pan, C.; Wang, Z. L. Tunable Tribotronic Dual-Gate Logic Devices Based on 2D MoS_2 and Black Phosphorus. *Adv. Mater.* **2018**, *30*, 1705088.
(37) Gao, A.; Lai, J.; Wang, Y.; Zhu, Z.; Zeng, J.; Yu, G.; Wang, N.; Chen, W.; Cao, T.; Hu, W.; Sun, D.; Chen, X.; Miao, F.; Shi, Y.; Wang, X. Observation of Ballistic Avalanche Phenomena in Nanoscale Vertical InSe/BP Heterostructures. *Nat. Nanotechnol.* **2019**, *14*, 217−222.
(38) Li, X.; Yang, L.; Si, M.; Li, S.; Huang, M.; Ye, P.; Wu, Y. Performance Potential and Limit of MoS_2 Transistors. *Adv. Mater.* **2015**, *27*, 1547−1552.
(39) Wan, D.; Abliz, A.; Su, M.; Liu, C.; Jiang, C.; Li, G.; Chen, H.; Guo, T.; Liu, X.; Liao, L. Low-Frequency Noise in High-Mobility a-InGaZnO/InSnO Nanowire Composite Thin-Film Transistors. *IEEE Electron Device Lett.* **2017**, *38*, 1540−1542.
(40) Li, L.; Liu, W.; Gao, A.; Zhao, Y.; Lu, Q.; Yu, L.; Wang, J.; Yu, L.; Shao, L.; Miao, F.; Shi, Y.; Xu, Y.; Wang, X. Plasmon Excited Ultrahot Carriers and Negative Differential Photoresponse in a Vertical Graphene van der Waals Heterostructure. *Nano Lett.* **2019**, *19*, 3295−3304.
(41) Wan, C.; Chen, G.; Fu, Y.; Wang, M.; Matsuhisa, N.; Pan, S.; Pan, L.; Yang, H.; Wan, Q.; Zhu, L.; Chen, X. An Artificial Sensory Neuron with Tactile Perceptual Learning. *Adv. Mater.* **2018**, *30*, 1801291.
(42) He, Y.; Nie, S.; Liu, R.; Jiang, S.; Shi, Y.; Wan, Q. Spatiotemporal Information Processing Emulated by Multiterminal Neuro-Transistor Networks. *Adv. Mater.* **2019**, *31*, 1900903.

https://dx.doi.org/10.1021/acsnano.0c03030
ACS Nano XXXX, XXX, XXX−XXX